Transport in Porous Media **1** (1986) 27–55.

Experimental and Numerical Analysis of Two-Phase Infiltration in a Partially Saturated Soil

JAOUDAT TOUMA AND MICHEL VAUCLIN
Institut de Mécanique de Grenoble, La CNRS No. 6, BP 68, F38402 Saint-Martin D'Heres Cédex, France

(Received: 29 May 1985; revised: 19 September 1985)

Abstract. The purpose of this study is to analyze the effects of the soil air flow on the process of water infiltration in a 93.5 cm deep vertical column for varied boundary conditions at the surface – positive time constant head; time constant fluxes smaller and greater than saturated soil hydraulic conductivity.

Several experiments conducted on a sandy soil column with and without a possible air flow through the wall are presented. Continuous and simultaneous measurements of water content and air and water pressure heads at different depths allow the analysis of the air and water movements within the soil and the determination of the capillary pressure and relative permeability for each phase as functions of the volumetric water content.

A numerical solution of the equations describing the simultaneous flow of air and water is compared with the experimental data and with the traditional one-phase flow modeling. The results show that the air movement may significantly affect water flow variables such as infiltration rates, water content profiles, and ponding times.

Furthermore, some basic assumptions used in two-phase flow modeling, such as the hydrodynamic stability of the wetting fronts and the pertinence of the relative permeability concept, are discussed in the light of the experimental data.

Key words. Multiphase flow, relative permeability, finite difference method, ponded water infiltration experiments, unsaturated flow.

1. Introduction

Traditional descriptions of water movement in the vadose zone neglect air effects by assuming that air is displaced without viscous resistance and is free to escape from the system. Such an assumption is common when analyzing, for instance, the infiltration of water into a soil profile (Philip, 1969). However, if the air flow is impeded by, for example, the presence of a shallow water table, an impermeable layer, or by lateral obstructions, significant reductions in infiltration rates may be observed, both in the field (Bianchi and Haskell, 1966; Dixon and Linden, 1972; Linden *et al.*, 1977; Starr *et al.*, 1978) and in laboratory columns (Powers, 1934; Free and Palmer, 1940; Horton, 1940; Wilson and Luthin, 1963; Peck, 1965a,b; Adrian and Franzini, 1966; MacWhorter, 1971; Vachaud *et al.*, 1973, 1974; Bond, 1978).

From a theoretical point of view, a survey of available literature shows that air and water movements in the unsaturated zone have been analyzed through the

two-phase flow approach classically used in petroleum reservoir engineering. This led to the development of either numerical (Brutsaert, 1970; Green *et al.*, 1970; Phuc and Morel-Seytoux, 1972; Watson and Curtis, 1975; Curtis and Watson, 1980; Mieri, 1981; Cushman, 1983) or quasi-analytical solutions (Brustkern and Morel-Seytoux, 1970; Noblanc and Morel-Seytoux, 1972; Morel-Seytoux and Khanji, 1974; Sonu and Morel-Seytoux, 1976; Nakano, 1981; Parlange *et al.*, 1982; Morel-Seytoux, 1982). The discussion about the pros and cons of these solutions is beyond the scope of this paper. Note only that most of the quasi-analytical solutions are based on the assumption of air incompressibility. This leads us to consider the total air and water velocity as constant in space.

It should be pointed out that most of these experimental and theoretical studies were conducted independently from one another. Very few attempts have been made to check the validity of the two-phase flow modeling by comparison with experimental data covering a large spectrum of initial and boundary conditions, classically encountered in either soil physics or hydrology.

The purpose of this study is, first, to report other experimental evidence of the air effects on water infiltration in a vertical soil column and, second, to test a numerical modeling, as general as possible, by comparing calculated and measured values for a large variety of boundary conditions.

2. Two-Phase Flow Equations

For isothermal flows in the vertical direction, the generalized Darcy's law for two immiscible fluids such as pure water and air may be written as

$$q_w = -\lambda_w\left(\frac{\partial p_w}{\partial z} - \rho_w g\right), \tag{1}$$

$$q_a = -\lambda_a\left(\frac{\partial p_a}{\partial z} - \rho_a g\right) \tag{2}$$

where q_w and q_a are the volumetric flux densities (LT^{-1}) of water and air, respectively, p_w and p_a are the fluid pressures ($ML^{-1}T^{-2}$), ρ_w and ρ_a are their specific masses (ML^{-3}), g is the acceleration of gravity (LT^{-2}) and z the vertical coordinate positively oriented downward.

The coefficients λ_w and λ_a are the fluid mobilities defined by

$$\lambda_w = \frac{kk_{rw}}{\mu_w} \quad \text{and} \quad \lambda_a = \frac{kk_{ra}}{\mu_a}, \tag{3}$$

where k is the intrinsic permeability (L^2) of the porous medium, k_{rw} and k_{ra} are the fluid relative permeabilities, and μ_w and μ_a the coefficients of the dynamic viscosity ($ML^{-1}T^{-1}$) of water and air, respectively.

The conservation of mass equation for both phases yields

$$\frac{\partial(\rho_w\theta_w)}{\partial t}+\frac{\partial(\rho_w q_w)}{\partial z}=0, \tag{4}$$

and

$$\frac{\partial(\rho_a\theta_a)}{\partial t}+\frac{\partial(\rho_a q_a)}{\partial z}=0, \tag{5}$$

where t is the time; θ_w and θ_a are the volumetric water and air contents, respectively. They are such that

$$\theta_w+\theta_a=n, \tag{6}$$

where n is the porosity which is time and space invariant for a nondeformable homogeneous medium.

Because air and water are immiscible fluids (air diffusion into water is neglected), there exists a pressure difference between the two fluids

$$p_a-p_w=p_c, \tag{7}$$

where p_c is the capillary pressure.

Assuming that water is incompressible and air is a perfect gas, the state equations for both fluids can be written as

$$\rho_i=\rho_{0i}\left(\frac{p_i}{p_0}\right)^m \tag{8}$$

where ρ_{0i} is the specific mass of the fluid i at the atmospheric pressure p_0, $m=0$ for water ($i\equiv w$) and $m=1$ for air ($i\equiv a$).

By expressing the fluid pressure in terms of water pressure heads relative to the atmospheric pressure

$$h_w=\frac{p_w-p_0}{\rho_{0w}g}; \qquad h_a=\frac{p_a-p_0}{\rho_{0w}g}, \tag{9}$$

Equations (1), (2), (7) and (8) take the equivalent forms

$$q_w=-K_w\left(\frac{\partial h_w}{\partial z}-1\right), \tag{10a}$$

$$q_a=-K_a\left(\frac{\partial h_a}{\partial z}-\frac{\rho_a}{\rho_{0w}}\right), \tag{10b}$$

$$h_a-h_w=h_c, \tag{10c}$$

$$\rho_i=\rho_{0i}\left(1+\frac{h_i}{h_0}\right)^m, \tag{10d}$$

where $K_w=\rho_{0w}g\lambda_w$ is the water conductivity (LT^{-1}) and $K_a=\rho_{0w}g\lambda_a$ is the air conductivity (LT^{-1}), both being functions of the water content θ_w.

In Equation (10d), h_0 is the atmospheric pressure expressed in terms of the water column height.

2.1. WATER PHASE PARTIAL DIFFERENTIAL EQUATION

Inserting Equation (10a) into (4), with $\rho_w = \rho_{0w}$, yields

$$\frac{\partial \theta_w}{\partial t} = \frac{\partial}{\partial z}\left\{ K_w\left(\frac{\partial h_w}{\partial z} - 1\right)\right\}. \tag{11}$$

By assuming that h_c is a unique function of θ_w (hysteresis and dynamic effects are neglected), the left-hand side member of Equation (11) can also be written as

$$\frac{\partial \theta_w}{\partial t} = C_w \cdot \frac{\partial h_c}{\partial t} = C_w\left(\frac{\partial h_a}{\partial t} - \frac{\partial h_w}{\partial t}\right), \tag{12}$$

where $C_w = \mathrm{d}\theta_w/\mathrm{d}h_c$ is the capillary capacity (L^{-1}) which is a function of θ_w. Then Equation (11) becomes

$$C_w\left(\frac{\partial h_a}{\partial t} - \frac{\partial h_w}{\partial t}\right) = \frac{\partial}{\partial z}\left\{ K_w\left(\frac{\partial h_w}{\partial z} - 1\right)\right\} \tag{13}$$

2.2. AIR PHASE PARTIAL DIFFERENTIAL EQUATION

Inserting Equation (10b) into (5) gives

$$\frac{\partial(\rho_a \theta_a)}{\partial t} = \frac{\partial}{\partial z}\left\{ \rho_a K_a\left(\frac{\partial h_a}{\partial z} - \frac{\rho_a}{\rho_{0w}}\right)\right\}. \tag{14}$$

Substitution of θ_a and ρ_a given by Equations (6) and (10d) into the left-hand side of Equation (14), combined with Equation (12), leads to

$$\left\{(n - \theta_w)\frac{\rho_{0a}}{h_0} - \rho_a C_w\right\}\frac{\partial h_a}{\partial t} + \rho_a C_w \frac{\partial h_w}{\partial t} = \frac{\partial}{\partial z}\left\{ \rho_a K_a\left(\frac{\partial h_a}{\partial z} - \frac{\rho_a}{\rho_{0w}}\right)\right\} \tag{15}$$

Equations (13), (15) and (10d) (with $i \equiv a$ and $m = 1$) describe the isothermal coupled air and water movements in an unsaturated, nondeformable and homogeneous porous medium. No other approximations are involved in these equations.

Assuming that the soil air phase is continuously (both in time and space) connected to the external atmospheric pressure, leads to $h_a \equiv 0$ and $h_c \equiv -h_w$.

Thus, Equation (13) becomes

$$C_w \frac{\partial h_w}{\partial t} = \frac{\partial}{\partial z}\left\{ K_w\left(\frac{\partial h_w}{\partial z} - 1\right)\right\} \tag{16}$$

with $C_w = \mathrm{d}\theta_w/\mathrm{d}h_w$, which is the classical well-known Richards' equation.

3. Material and Methods

Infiltration experiments were performed on a vertical column of sand packed into an acrylic plastic cylinder 93.5 cm high and with a 6 cm inside diameter. The bottom of the column was provided with a fritted stainless steel porous plate allowing it to be connected to an outer piezometric level.

The time changes of volumetric water contents at different depths were measured by attenuation of gamma rays emitted by an 241 Am, 100 mCr source. The source and the detector were mounted on a moving carriage, as described by Vachaud and Thony (1971).

The fluid pressure heads were measured at six depths ($z = 7$, 22, 37, 52, 67 and 82 cm). Each section was provided with two tensiometers diametrically opposed. The first one was a porous ceramic cup (air entry pressure of -1000 cm of water) for water pressure measurements. The second was a porous polyethylene disk (water entry pressure of 2 cm of water) permeable to air and impervious to water, for air pressure measurements. Each tensiometer was connected to its own differential pressure transducer.

Compared with the previous experiments of Vachaud *et al.* (1973, 1974), this method has the great advantage of avoiding the use of hypodermic needles, which saturate when the relative water pressure head approaches zero. Another advantage is the independent measurement of pressure for each phase, without using a scannivalve in which the measurement of the pressure of one phase might be influenced by the pressure of the other.

The column has no lateral openings other than those destined for the tensiometric measurements. The measuring sequence was basically the same as that described by Vachaud and Thony (1971) with the transducer readings, gamma counts, the position of the carriage recorded at the end of each counting sequence (60 s), and the automatic displacement of the carriage to the next prescribed location.

The soil used was an alluvional coarse sand. It was washed to prevent suspended fine material from moving during air and water flows. The resulting granulometry ranged between 0.02 and 1 mm with 50% of its weight less than 0.3 mm. The air-dried sand was packed into the column as uniformly as possible. The bulk density profile determined by gamma-ray attenuation led to a mean value of 1.67 ± 0.01 g/cm^3, and a mean porosity $n = 0.37$ cm^3/cm^3.

The soil surface was protected by a fine metallic grid with negligible impedance to prevent any modification in the soil structure near the surface during the infiltration experiments, mainly, when air escapes.

In order to show the influence of the air phase on the mechanism of water infiltration, two types of experiments were conducted with the same initial and boundary conditions:

(a) *Type A*: *bounded column*. All the pressure transducers being mounted, the column is laterally sealed, and the only possibility for the air to escape is through

the soil surface, because the bottom of the column is also isolated from the piezometric level by a valve.

(b) *Type B*: *open column*. The air pressure transducers being removed, the soil air is in contact with the external atmosphere through corresponding tensiometers. The bottom of the column is connected to the external piezometric level.

For each type, three experiments were performed:

(i) Time constant positive water head $h_w(0, t) = 2.3$ cm was imposed at the surface by a Mariotte bottle device. This corresponds to ponded infiltration.

(ii) Time constant water flux $q_w(0, t) = 8.3$ cm/h smaller than the saturated hydraulic conductivity (K_{ws}) was applied at the surface. A nonponded infiltration regime may be expected.

(iii) Time constant water flux $q_w(0, t) = 20$ cm/h greater than K_{ws} was applied at the surface. In this case, pre-ponding, ponding and post-ponding situations, as described by Rubin and Steinhardt (1963), through the one-phase flow approach may be expected.

In the flux infiltration experiments, water was supplied at the surface by means of a volumetric pump through a series of 20 hypodermic needles (0.7 mm inner diameter) regularly distributed over the surface of the soil column.

The experiments of infiltration were run after the first saturation of the soil column and the subsequent first drainage up to the static equilibrium corresponding to a piezometric level at 120 cm below the surface.

The initial condition of each infiltration was obtained by draining the sand column to the same piezometric level.

All the experimental tests were run at room temperature, 20 ± 1°C.

4. Experimental Results

Before embarking on the analysis of the results, the soil air and water hydrodynamic characteristics are presented.

4.1. SOIL CHARACTERISTICS

4.1.1. *Intrinsic Permeability*

The intrinsic permeability of the medium was determined first by applying constant fluxes of air q_a at the bottom of the dry sand column until permanent flows were obtained. The corresponding air pressure heads h_a were recorded at six depths. An example is given in Figure 1a for $q_a = 286$ cm/h. Seventeen such experiments were run for q_a, ranging from 61 to 398 cm/h. The air flow rates were measured by a sensitive rotameter. Figure 1b gives the experimental

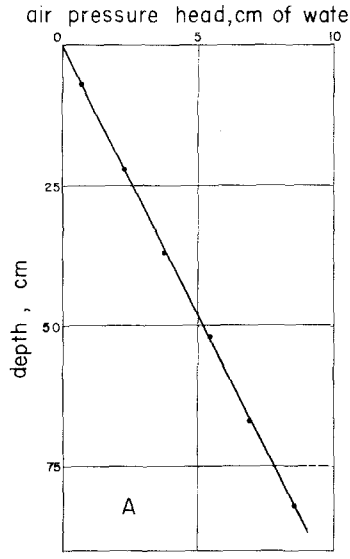

Fig. 1a. Typical profile of air pressure head for $q_a = 286$ cm/h applied at the bottom of the dry soil column.

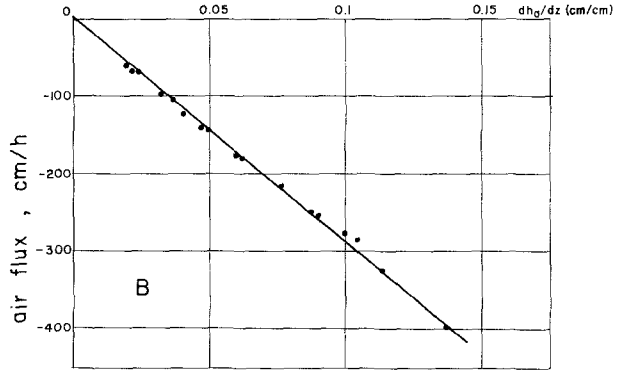

Fig. 1b. Gradient of air pressure head as a function of volumetric air flux in the dry soil column. Points are the experimental values. Solid line corresponds to the linear regression.

relation between q_a and the gradient of air pressure head. No deviation from Darcy's law (Equation 10b) could be observed. Thus, the statistical regression between q_a and dh_a/dz leads to a air saturated conductivity value of $K_{as} = 2800 \pm 30$ cm/h with a correlation coefficient $r = 0.998$. The intrinsic permeability inferred from $K_{as} = k\rho_{0w}g/\mu_a$, is $k = (1.45 \pm 0.02) \times 10^{-7}$ cm^2. (At the temperature of 20°C, $\mu_a = 1.83 \times 10^{-4}$ poise.)

4.1.2. *Capillary Pressure – Water Content Relationship*

The water contents and air and water pressure heads recorded during ponded infiltration tests yielded the capillary pressure head h_c (Equation 10c) as a

function of water content shown in Figure 2. No distinction can be made either between points inferred from experiments performed on the open (open circles) and bounded (solid circles) columns, or from depth to depth.

The analytical expression (Van Genuchten, 1980)

$$\theta_w = \frac{\theta_{ws} - \theta_{wr}}{|1 + (\alpha h_c)^{\beta}|^{\gamma}} + \theta_{wr} \tag{17}$$

was fitted to the experimental data. Statistical treatment gave the following values

$$\theta_{ws} = 0.312 \text{ cm}^3/\text{cm}^3; \qquad \theta_{wr} = 0.0265 \text{ cm}^3/\text{cm}^3;$$

$$\alpha = 0.044 \text{ cm}^{-1}; \qquad \beta = 2.2 \quad \text{and} \quad \gamma = 1 - 1/\beta = 0.55.$$

It should be noted that, due to air entrapment, the natural water saturation θ_{ws} is significantly smaller than the porosity $n = 0.37 \text{ cm}^3/\text{cm}^3$.

Furthermore, θ_{wr} has to be viewed here only as a fitting parameter and not necessarily as the actual residual water content.

In addition, points obtained during drainage experiments performed between

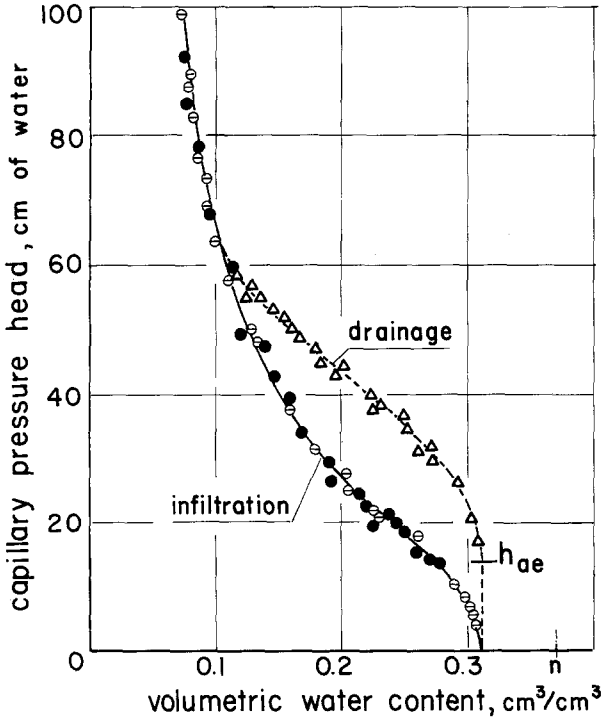

Fig. 2. Capillary pressure head – water content relationship – measured during ponded infiltration in the open (θ) and bounded (●) columns, and during drainage of the open column (△). The solid line corresponds to the analytical expression (Equation (17)).

two infiltrations are reported (triangles) in Figure 2. It appears that significant hysteresis effects may be expected for a water content greater than 0.11 cm^3/cm^3.

The air entry pressure on the draining curve is estimated at $h_{ae} = 14$ cm of water.

4.1.3. *Air and Water Conductivities*

The water conductivity values $K_w(\theta_w)$ were classically obtained by applying the instantaneous profile method (Watson, 1966) to the transient ponded infiltration data.

For the determination of the air conductivity values $K_a(\theta_w)$, a flow of air ($q_a = 334$ cm/h) was imposed at the bottom of the wet soil column, laterally bounded until the establishment of the permanent flow regime. The corresponding air pressure head and moisure content profiles (Figure 3) gave both the air pressure gradient and water content at each depth of measurement. Then $K_a(\theta_w)$ were calculated by using Darcy's law (Equation 10b). The results are presented in Figure 4 for the relative permeabilities of each phase: $k_{ra} = K_a/K_{as}$ and $k_{rw} = K_w\mu_w/K_{as}\mu_a$.

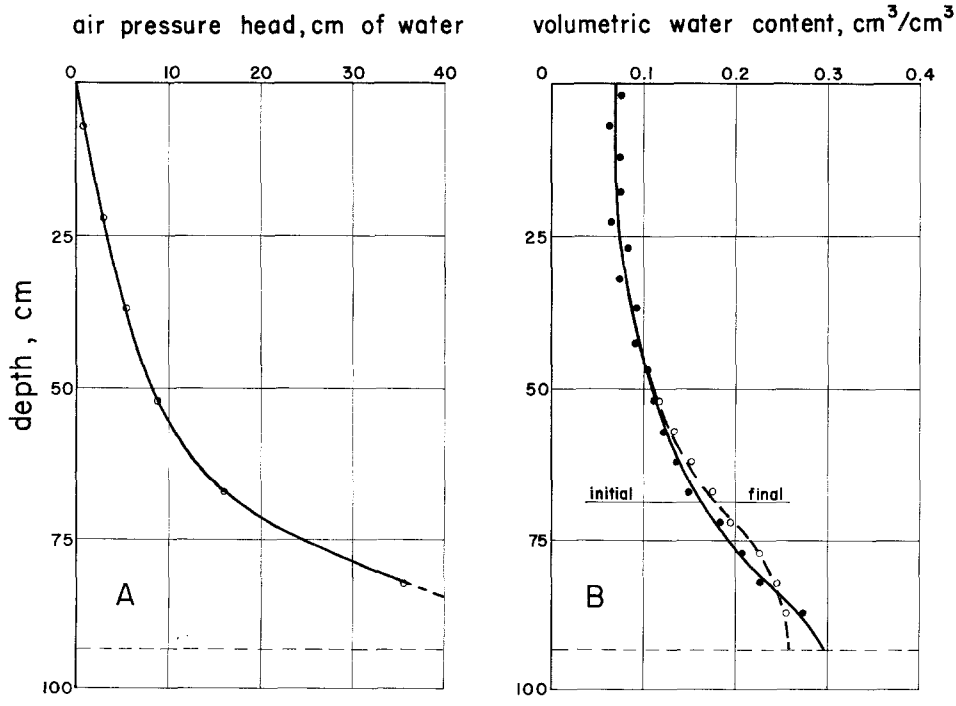

Fig. 3. Experimental air pressure head (3a) and water content (3b) profiles corresponding to a permanent air flow $q_a = 334$ cm/h.

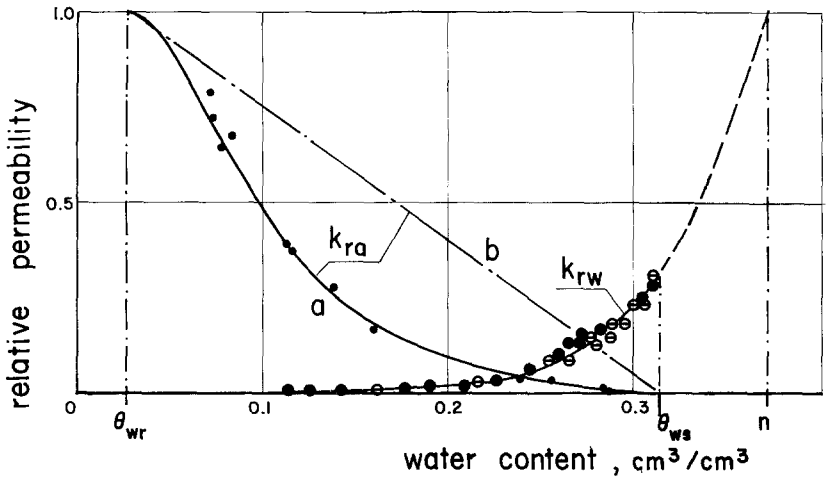

Fig. 4. Relative permeabilities as functions of water content. Open and solid circles correspond to data obtained in the open and bounded columns, respectively. Solid lines correspond to the analytical expression given in the text. Curb (b) represents the hypothetical linear relation $k_{ra}(\theta_w)$.

The following comments can be made:

(i) In the determination of $k_{rw}(\theta_w)$, no distinction can be made between infiltration experiments run in the open and bounded columns. Note also that the presence of a residual air phase ($\theta_{ar} = n - \theta_{ws} = 0.058\ \text{cm}^3/\text{cm}^3$) induces a drastic reduction of k_{rw} from 1.0 for the hypothetical full saturation to 0.31 at the natural one.

(ii) The $k_{ra}(\theta_w)$ values at high water content values are relatively crude because of experimental uncertainties in the determination of the air pressure gradient (Figure 3a). It should be noted that another similar experiment with $q_a = 61$ cm/h gave air conductivity values similar to those presented in Figure 4.

(iii) For modeling purposes, the following analytical expressions have been fitted to the experimental data

$$K_w = A_w \cdot \theta_w B_w \tag{18}$$

with $A_w = 18\,130$ cm/h and $B_w = 6.07$.

This leads to $K_{ws} = 15.40$ cm/h

$$K_a = K_{as} \cdot \frac{A_a}{A_a + h_c B_a} \tag{19}$$

with $A_a = 3.86 \times 10^{-5}$; $B_a = -2.4$ and $K_{as} = 2800$ cm/h.

4.2. PONDED EXPERIMENTS

Points in Figure 5 show the water-content profiles for the experiment in the open (5a) and the bounded columns (5b) obtained by smoothing the time-evolutions of

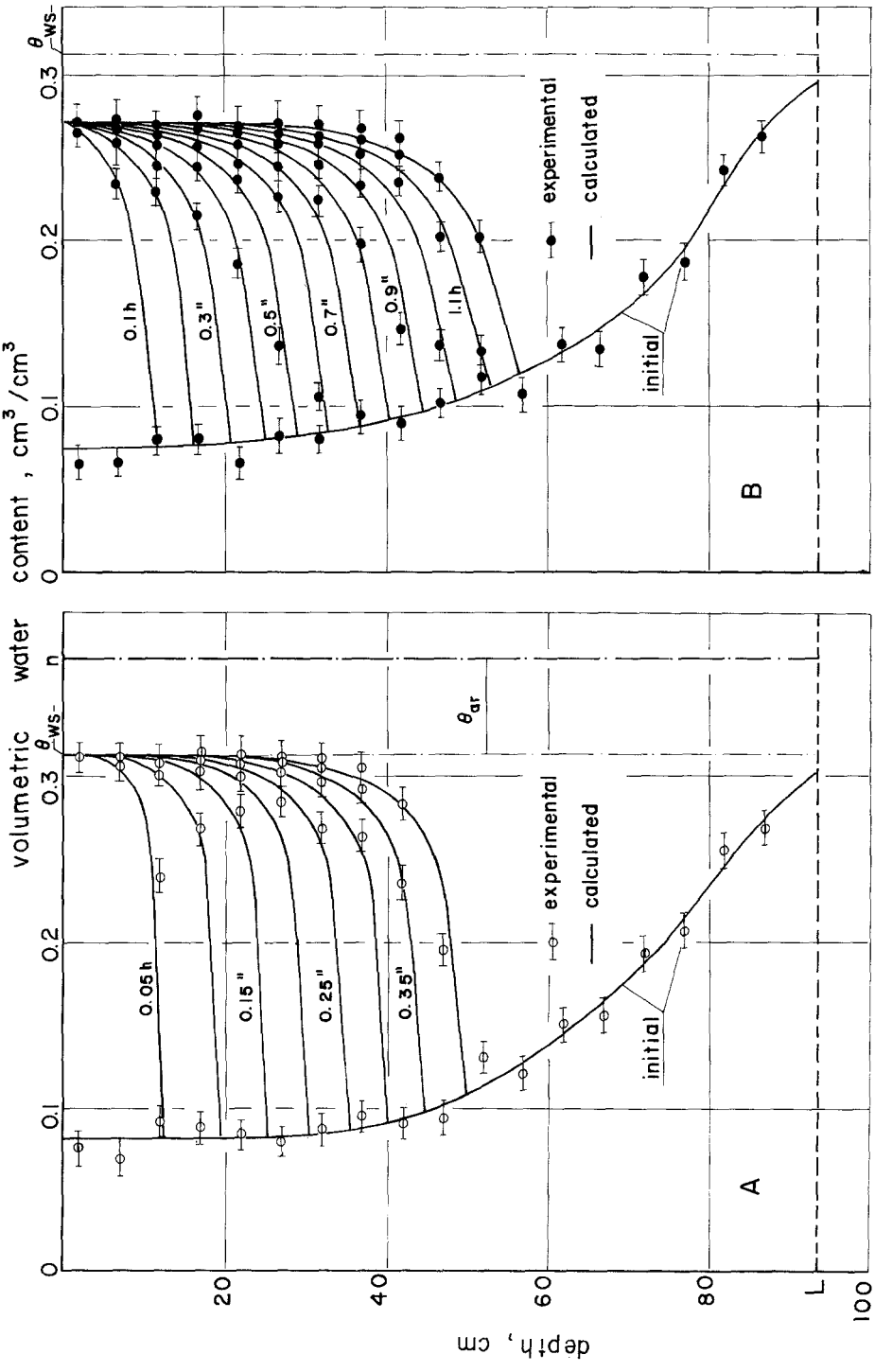

Fig. 5. Ponded infiltration: water content profiles in the open (5a) and bounded (5b) columns. Horizontal bars represent experimental uncertainties.

$\theta_w(t)$ measured at different depths. The horizontal bars correspond to the experimental uncertainties (assimilated to ±one standard deviation) associated with each value obtained by gamma-ray attenuation (Vauclin, 1971).

Figure 6 presents the cumulative water infiltration $I(t)$ (6a), as well as the infiltration rate $q_w(t) = \mathrm{d}I/\mathrm{d}t$ (6b) for the two experiments. Note that these values obtained from the Mariotte bottle readings agreed with the soil-water storage changes calculated by integrating the water content profiles.

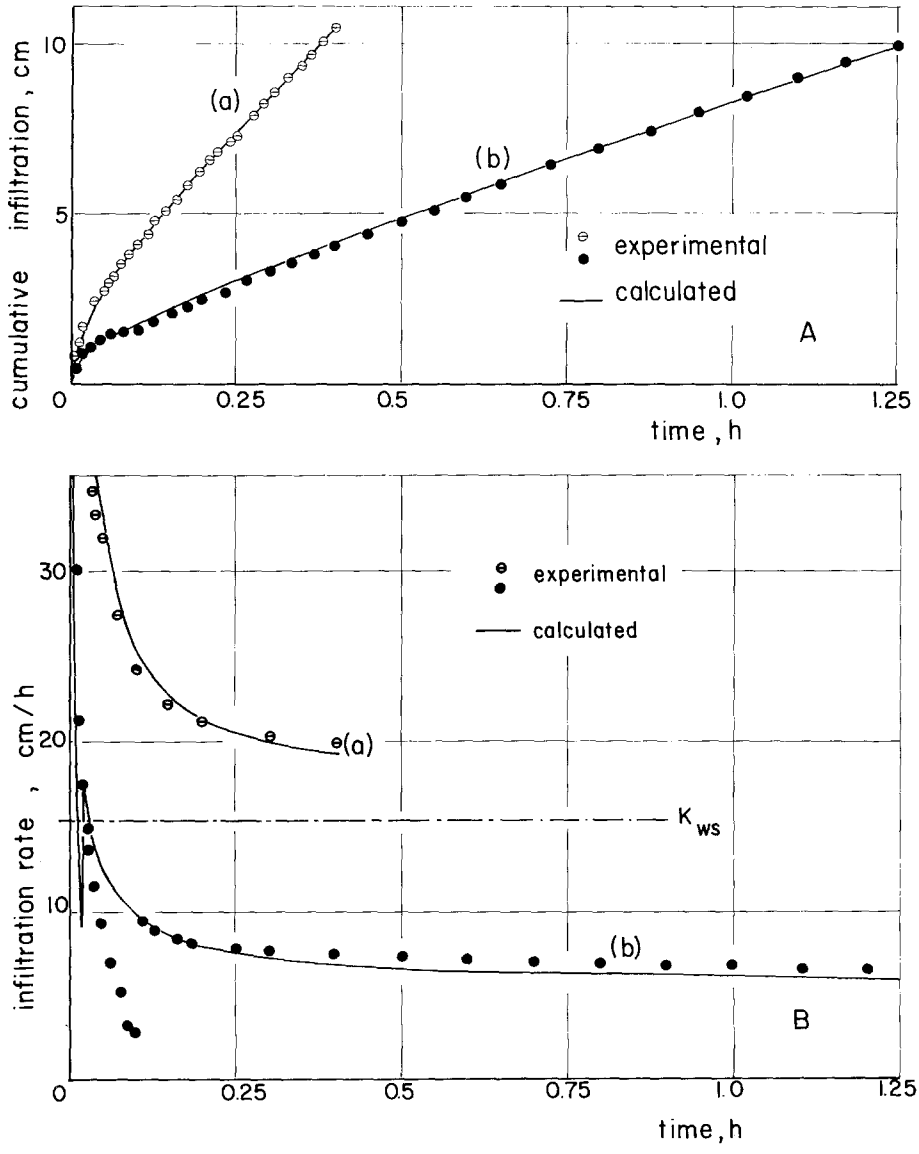

Fig. 6. Ponded infiltration: time evolution of cumulative infiltration (6a) and rate of infiltration (6b) in the open (curves (a)) and bounded (curves (b)) columns.

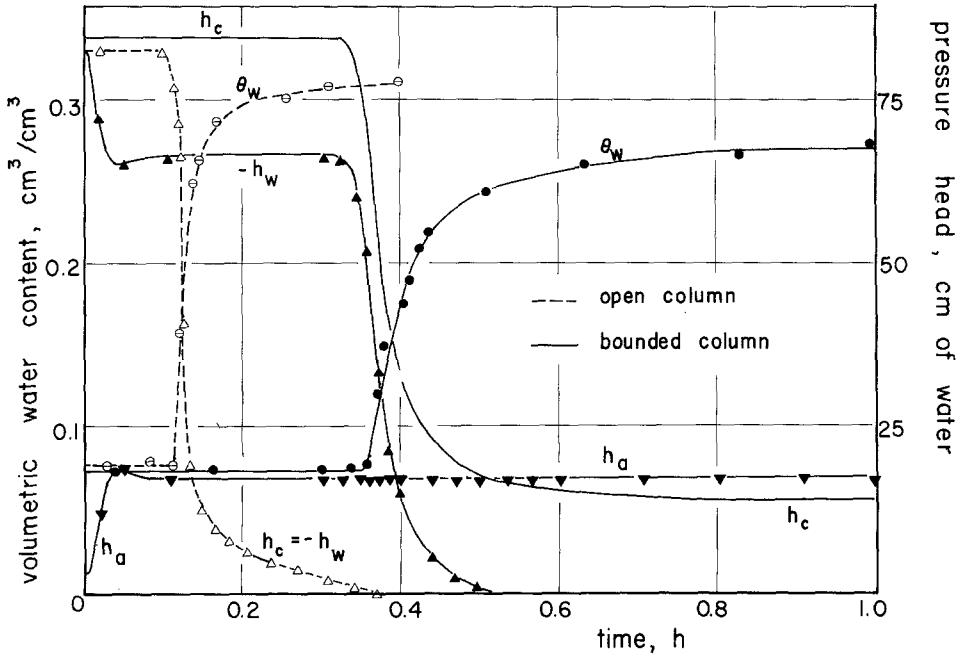

Fig. 7. Ponded infiltration: time evolution of air (h_a); water (h_w), capillary (h_c) pressure heads and of water content (θ_w) at $z = 22$ cm. Open and solid symbols correspond to the open and bounded columns, respectively.

In addition, Figure 7 presents as an example, the time evolution of h_c, h_w, h_a and θ_w measured at a particular depth ($z = 22$ cm) for both experiments.

Three major differences between the profiles of Figures 5a (open column) and 5b (bounded column) are observed. The first difference is the rate of advance of the wetting front, which is drastically reduced when air cannot escape laterally. This is consistent with the cumulative infiltration data shown in Figure 6a. Second, the slopes are less abrupt when air must escape through the soil surface (Figure 5b) as described by Youngs and Peck (1964) and Parlange and Hill (1979). Third, the steady-state water content profile which corresponds to the natural saturation (0.312 cm^3/cm^3) in Figure 5a, is only $\theta_w(z) = 0.272$ cm^3/cm^3 in Figure 5b.

Although both the theoretical analysis of Youngs and Peck (1964) and the numerical modeling of Phuc and Morel-Seytoux (1972) predict, in the latter case, a drainage near the surface in the early stage of infiltration, it was not possible to measure such a drainage by gamma-ray attenuation.

For the experiment in the bounded column when water begins to infiltrate, the air in the soil pores is pushed aside to make room for water and its pressure builds up, as is shown in Figure 7 for $z = 22$ cm. The water pressure head varies in the opposite direction in such a way that the capillary pressure remains unchanged

from its initial value, as long as the wetting front has not reached this depth. The same behaviour for all depths was observed.

It should be noted that air pressures recorded at various depths at a given time, were not significantly different from each other (less than 0.5 cm of water, which corresponds to the accuracy of the measurement). Then it can be speculated that only the air compression ahead of the wetting front, and not the viscous resistance to airflow, affects the water infiltration. This air compression leads to a slowing down of the infiltration rate, as is clearly shown in Figure 6b. For instance, at $t = 0.1$ h, the flux entering the surface is six times less than saturated water conductivity K_{ws} and 10 times less than the infiltration rate when air is free to laterally escape.

It may be speculated that the sudden drop in h_a at $t = 0.1$ h (Figure 7), which has been observed simultaneously at all depths, may be the result of air forcing its way through the soil matrix and creating new passages with less resistance to air motion. This singularity, which corresponds to the change in the slope of $I(t)$ (Figure 6a), does not necessarily mean that the air counterflow begins at this time, as assumed in the numerical modeling of Noblanc and Morel-Seytoux (1972).

As a matter of fact, the air must escape through the surface as soon as its pressure reaches a critical value $h_{a_{crit}} = h_{ae} + 2.3$ cm, where h_{ae} is 14 cm of water (Figure 2). For this value, the cumulative infiltrated water is given by

$$I_{crit} = \frac{h_{a_{crit}} \int_0^L \{n - \theta_{wn}(z)\}\, dz}{h_0 + h_{a_{crit}}} \tag{20}$$

where $\theta_{wn}(z)$ is the initial water content profile and h_0 is the atmospheric pressure head. This equation is obtained by applying the perfect gas law at the air phase initially present in the soil profile. For $h_{a_{crit}} = 16.3$ cm and $h_0 = 1033$ cm of water, Equation (20) gives $I_{crit} = 0.36$ cm, and the corresponding time is $t_{crit} = 12$ s. It should be noted that the visual observations showed that air began to bubble through the free surface very soon (around 10 s) after the beginning of the water application.

As time progresses, the stabilization of air pressure heads at all depths around a sill of about 17 cm of water, tends to demonstrate that the air head losses are quite insignificant along the column.

4.3. FLUX EXPERIMENTS

4.3.1. *Flux Less than K_{ws}*

Figure 8 presents the water content profiles corresponding to the infiltration under a time constant $q_w(0, t) = 8.3$ cm/h applied at the soil surface. The points correspond to the experiments run in the open, and the bounded column as well. In the latter case, air pressure recordings did not show any significant differences (less than a few millimeters of water) from the atmospheric value. Because

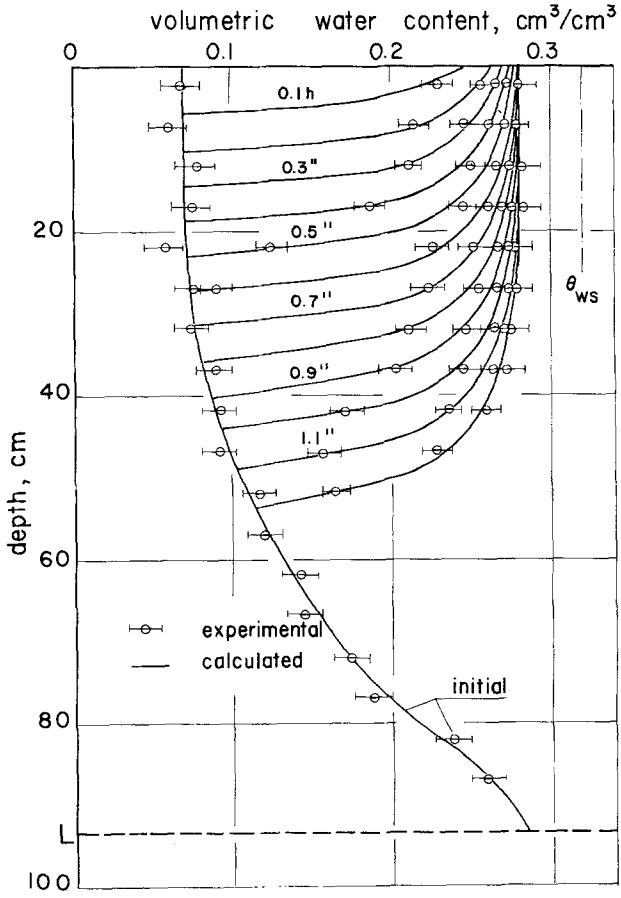

Fig. 8. Infiltration at $q_w(0, t) = 8.3$ cm/h: time evolution of water content profiles. Horizontal bars correspond to uncertainties associated with the measurements.

$q_w(0, t)$ is less than K_{ws}, no water saturation of the surface occurs and air is free to escape through it. Note that in both cases, the steady-state water content profile measured near the surface agrees very well with the theoretical one given by $q_w(0, t) = K_w(\theta_l)$ which leads to $\theta_l = 0.282$ cm³/cm³.

4.3.2. *Flux Higher than* K_{ws}

The points in Figure 9 shows the measured water content profiles for the infiltration in the open (9a) and bounded (9b) columns. The points in Figure 10 present the corresponding cumulative water infiltration as a function of time. The values were obtained by integrating the water content profiles. In addition, the points in Figure 11 give the time evolution of the mean air pressure head measured during the experiment run in the bounded column.

When air can escape laterally from the column, the results (Figures 9a and 10a) agree well with those which are expected by the traditional one-phase flow

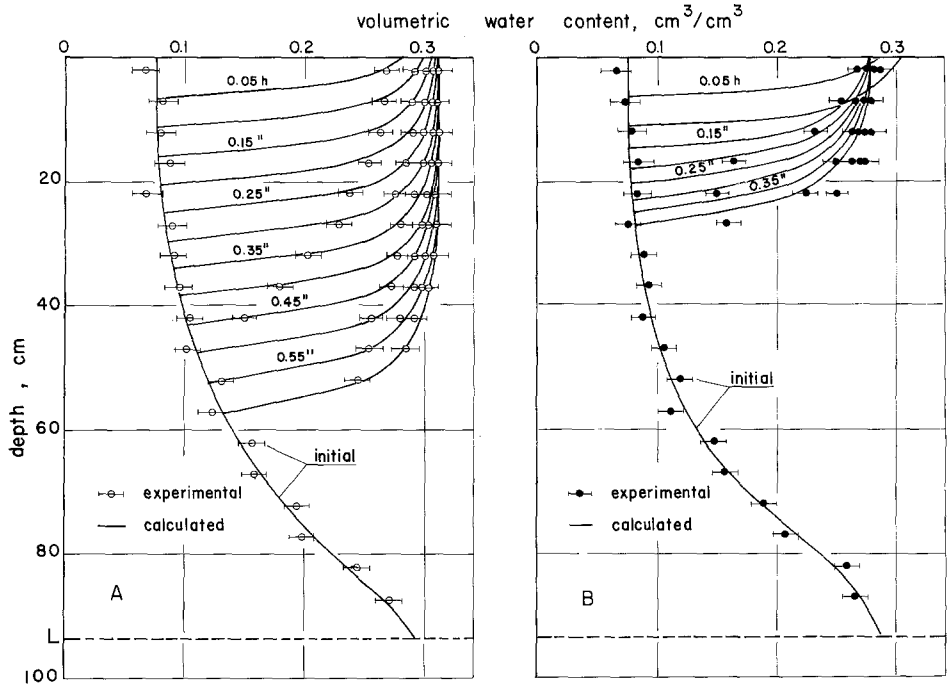

Fig. 9. Infiltration at $q_w(0, t) = 20$ cm/h: water content profiles in the open (9a) and bounded (9b) columns. Horizontal bars correspond to experimental uncertainties associated with the measurements.

approach: the surface-water content is an increasing function of time until saturation $\theta_{ws} = 0.312\ \text{cm}^3/\text{cm}^3$ is attained, infiltration ($\text{d}I/\text{d}t$) and the water supply ($q_w(0, t)$) rates are equal (Figure 10a). After the ponding of the surface, the infiltration rate becomes less than $q_w(0, t)$. From visual inspection, the ponding time was about $t_p = 0.38$ h.

For the experiment conducted in the bounded column, the same phenomenon as before seemed to be observed for times smaller than $t = 0.08$ h: no air compression was measured (Figure 11) and water content profiles and cumulative infiltration are similar in both experiments. Air can escape through the surface, because the water saturation of the soil has not yet been reached.

At $t = 0.08$ h, the air is significantly compressed in the medium (Figure 11), probably because not enough passages are available for the air to escape freely through the surface. Ponding of the surface was observed at about $t_p = 0.14$ h. This time more or less corresponds to both the maximum of h_a (Figure 11) and the beginning of a significant decrease of the infiltration rate (Figure 10b). At this time and later on, the water content near the surface (Figure 9b) is about the same as the value observed for the ponding infiltration in the bounded column. Note also that the sills reached by h_a (Figures 7 and 11) are about the same in both experiments.

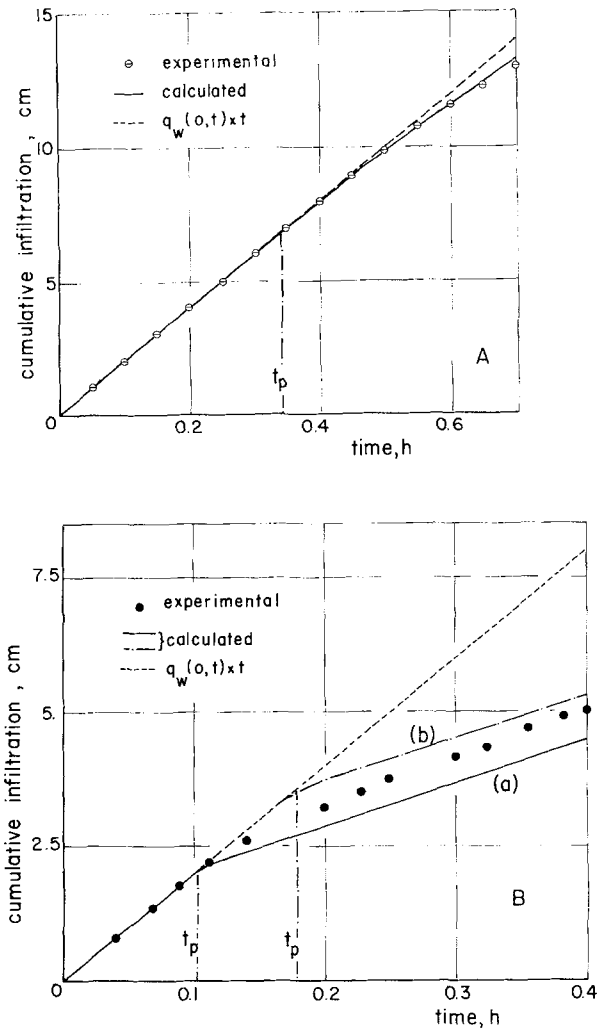

Fig. 10. Infiltration at $q_w(0, t) = 20$ cm/h: time evolution of cumulative infiltration in the open (10a) and bounded (10b) columns. Dotted lines represent the cumulative amount of water supply. t_p is the ponding time. Curves (a) and (b) correspond to the measured and linear relation $k_{ra}(\theta_w)$, respectively.

More detailed comments will be made later on by comparing experimental and numerical results.

5. Numerical Modeling

Because Equations (13) and (15) are nonlinear parabolic partial differential equations, no exact analytical solutions are known. Here, they have been simultaneously solved by an implicit finite difference scheme. The linearization – estimation of C_w, K_w, ρ_a, K_a in time – is explicit. The internodal air and water

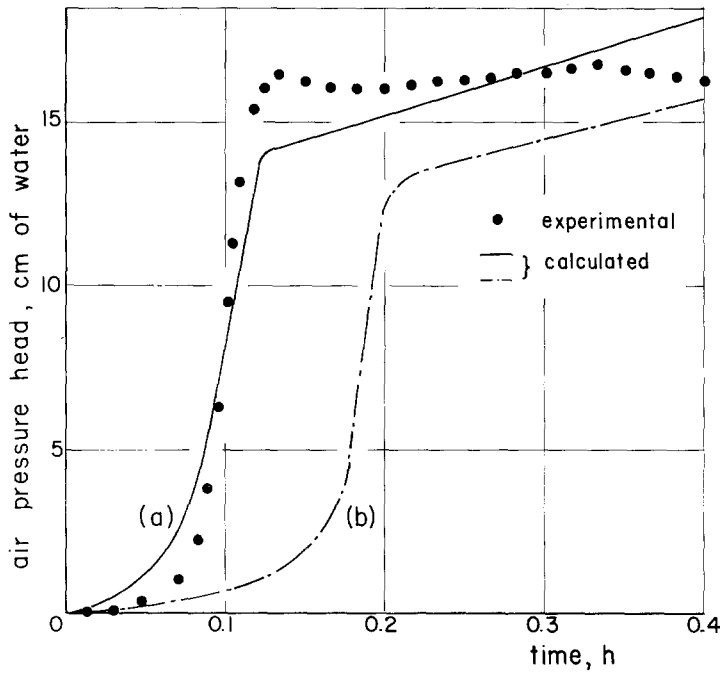

Fig. 11. Infiltration at $q_w(0, t) = 20$ cm/h in the bounded column: time evolution of the mean air pressure head. Curves (a) and (b) correspond to the measured and linear relation $k_{ra}(\theta_w)$, respectively.

conductivities are calculated by the geometric average of the nodal values (Haverkamp and Vauclin, 1979).

The resulting linear system has been solved by a modified Thomas algorithm similar to that used by Douglas *et al.* (1959). More details can be found in Touma (1984).

All the experiments previously presented have been simulated with a space step $\Delta z = 1$ cm and time step $\Delta t = 1$ s. These values gave a fair compromise between numerical stability and accuracy requirements, and acceptable computational cost. Note that only Equation (16) was solved to simulate the experiments in the open column.

The boundary conditions which have been used to simulate the experiments are summarized in Tables I and II, for the infiltrations run in the bounded (type A) and open (type B) columns, respectively. Dealing with the experiments of types A and B, with $q_w(0, t) = 20$ cm/h, the ponding time is numerically defined as $h_w(0, t_p) = 0$. For the infiltrations (both ponding and flux $q_w(0, t) = 20$ cm/h) run in the bounded column (Table I), t_{crit} is defined as the time value for which air begins to escape through the surface. At this time, the Neumann condition of no air flow at the surface is changed into a Dirichlet condition of either a constant air pressure for the ponding infiltration or a time variable air pressure $h_a(0, t) =$

Table I. Boundary conditions used in the modeling of the experiments run in the bounded column

Experiments	Boundary conditions	
	$z = 0$	$z = L = 93.5$ cm
(a) *Ponded infiltration*	$h_w(0, t) = 2.3$ cm	$-K_w\left(\frac{\partial h_w}{\partial z} - 1\right) = 0$
	$-K_a\left(\frac{\partial h_a}{\partial z} - \frac{\rho_a}{\rho_{0w}}\right) = 0$ for $0 \leq t \leq t_{crit}$ $h_a(0, t) = h_{ae} + 2.3$ for $t > t_{crit}$	$-K_a\left(\frac{\partial h_a}{\partial z} - \frac{\rho_a}{\rho_{0w}}\right) = 0$
(b) *Flux infiltration*		
(i) $q_w(0, t) = 8.3$ cm/h	$-K_w\left(\frac{\partial h_w}{\partial z} - 1\right) = 8.3$	$-K_w\left(\frac{\partial h_w}{\partial z} - 1\right) = 0$
	$h_a(0, t) = 0$	$-K_a\left(\frac{\partial h_a}{\partial z} - \frac{\rho_a}{\rho_{0w}}\right) = 0$
(ii) $q_w(0, t) = 20$ cm/h	$-K_w\left(\frac{\partial h_w}{\partial z} - 1\right) = 20$ for $0 \leq t \leq t_p$ $h_w(0, t) = q_w(0, t)t - I(t)$ for $t > t_p$	$-K_w\left(\frac{\partial h_w}{\partial z} - 1\right) = 0$
	$h_a(0, t) = 0$ for $0 \leq t \leq t_p$ $-K_a\left(\frac{\partial h_a}{\partial z} - \frac{\rho_a}{\rho_{0w}}\right) = 0$ for $t_p < t \leq t_{crit}$ $h_a(0, t) = h_{ae} + h_w(0, t)$ for $t > t_{crit}$	$-K_a\left(\frac{\partial h_a}{\partial z} - \frac{\rho_a}{\rho_{0w}}\right) = 0$

Table II. Boundary conditions used in the modeling of the experiments run in the open column

Experiments	Boundary conditions	
	$z = 0$	$z = L = 93.5$ cm
(a) *Ponded infiltration*	$h_w(0, t) = 2.3$ cm	$h_w(L, t) = h_w(L, 0) = -5.8$ cm
(b) *Flux infiltration*		
(i) $q_w(0, t) = 8.3$ cm/h	$-K_w\left(\frac{\partial h_w}{\partial z} - 1\right) = 8.3$	$h_w(L, t) = h_w(L, 0) = -9.9$ cm
(ii) $q_w(0, t) = 20$ cm/h	$-K_w\left(\frac{\partial h_w}{\partial z} - 1\right) = 20$ for $0 \leq t \leq t_p$ $h_w(0, t) = q_w(0, t)t - I(t)$ for $t > t_p$	$h_w(L, t) = h_w(L, 0) = -8.7$ cm

$h_{ae} + h_w(0, t)$ for the infiltration with $q_w(0, t) = 20$ cm/h. In the latter case, $h_w(0, t)$ is numerically calculated through the mass conservation equation

$$h_w(0, t) = W(t) - I(t), \tag{21}$$

where $W(t) = q_w(0, t)$. t is the amount of water supplied at the surface and $I(t) = \int_0^L \{\theta_w(z, t) - \theta_{wn}(z)\}\, dz$ is the cumulative infiltration depth estimated as the change in water storage in the soil.

Note that this equation was also used to predict the time evolution of the water depth after the ponding of the surface for the infiltration with $q_w(0, t) = 20$ cm/h in the open column (Table II).

For the simulation of the experiments of types A and B, the initial water flow conditions are the water pressure heads calculated from the observed water content profiles. For the simulation of type A experiments, the soil air phase is considered to be initially at the atmospheric pressure ($h_{an}(z) = 0$) within the whole column.

Before presenting the results it should be remembered that the soil properties were established from only data obtained during the ponded infiltrations. Thus, the numerical simulations for the other types of boundary conditions have to be viewed as predictions and tests of the modeling by comparing them with the corresponding experimental data.

A measure of the intrinsic performance in the numerical procedure can be obtained by comparing, at any time, less than t_p, the cumulative infiltration depth $I(t)$ and the cumulative amount of water supplied at the surface $W(t)$.

Table III gives some values of the mass balance criterion defined as

$$\eta(t) = \frac{I(t) - W(t)}{W(t)} \tag{22}$$

for the experiments (types A and B) run with flux-type surface conditions. A perfect conservative numerical scheme would correspond to $\eta(t) = 0$. One- and two-phase flow modelings give very similar, good ratios, except, maybe, at the early stages of the infiltration for which the two-phase flow simulations seem to be more accurate. At small times (i.e., $t \leq 0.10$ h) using a finer grid size ($\Delta t, \Delta z$), would lead to a better numerical mass conservation, but at higher computational costs.

For purposes of comparison with the experimental data, the numerical results are reported in Figures 5 and 6 for the ponded infiltration experiments, in Figure 8 ($q_w(0, t) = 8.3$ cm/h), and in Figures 9–11 ($q_w(0, t) = 20$ cm/h) for the flux infiltration experiments. In addition, Figure 12 presents typical air pressure head profiles calculated by the two-phase flow modeling for the three experiments (ponding and fluxes lesser and greater than K_{ws}) run in the bounded column. The values measured at six depths are also reported. Figure 13 displays the time-evolutions of the surface-water content $\theta_w(0, t)$, the infiltration rate dI/dt, and the water depth above the surface $k_w(0, t)$ calculated by the one- (open column)

Table III. Time evolution of the numerical mass-balance criterion expressed as a percentage.

Experiments		Time (h)						
		0.05	0.10	0.20	0.30	0.40	0.50	0.60
$q_w(0, t) = 8.3$ cm/h	Open column (one-phase flow)	−2.10	−1.00	−0.50	−0.31	−0.22	−0.15	−0.12
	Bounded column (two-phase flow)	1.13	0.78	0.56	0.46	0.40	0.37	0.34
$q_w(0, t) = 20$ cm/h	Open column (one-phase flow)	−2.80	−1.29	−0.54	−0.27	ponding of		
	Bounded column (two-phase flow)	1.65	1.18			the surface		

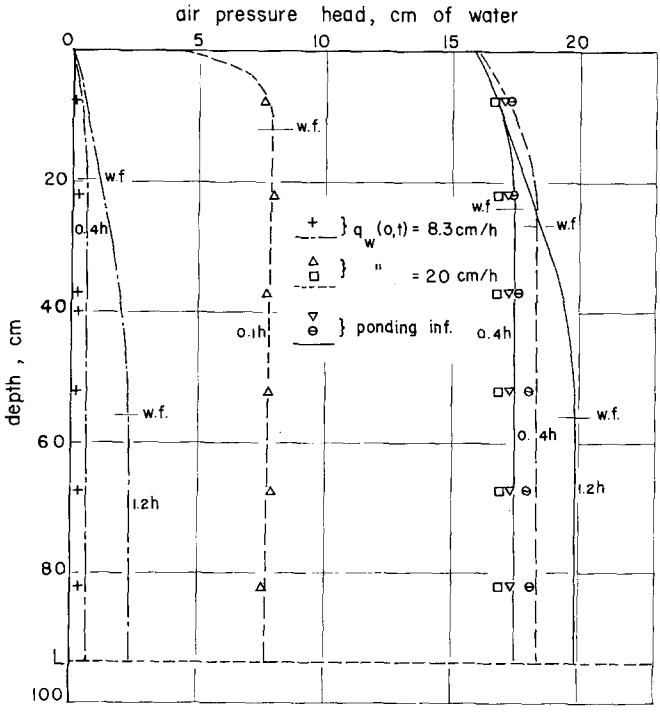

Figure 12. Air pressure head profiles measured and calculated by the two-phase flow approach. w.f. stands for wetting front.

and two- (bounded column) phase flow modelings for the infiltration with $q_w(0, t) = 20$ cm/h.

The main features are the following:

(1) A definite agreement between the measured and calculated values is observed for all the experiments run in the open column. Whatever the boundary conditions are, the one-phase flow approach seems to be adequate for modeling the infiltration when air can freely escape ahead of the wetting front. Note that these experiments were also simulated by the quasi-analytical flux-concentration approach (Philip, 1973). The corresponding results given in Boulier *et al.* (1984) agree very well with both the experimental data and one-phase flow numerical simulation (Equation (16)) presented here.

(2) Although very acceptable, the simulations of the experiments run in the bounded column (Equations 13 and 15) appear less satisfying, however, and more particularly for the infiltration with $q_w(0, t) = 20$ cm/h (Figures 9–12). As compared with the experimental values, the overestimation of the calculated air pressure heads at the early stages of the infiltration (Figure 11, curve (a)) provokes an underestimation of the ponding time (while t_p was visually observed at 0.14 h, the calculated value is $t_p = 0.10$ h) which, consequently, leads to cumulative infiltration depths of 10% less than the measured ones (Figure 10b,

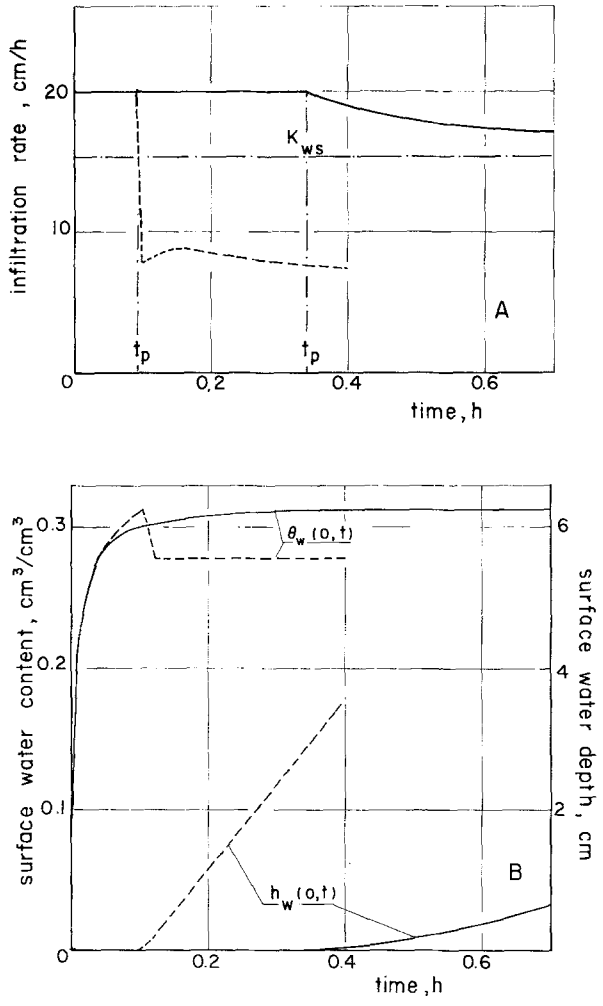

Fig. 13. Infiltration at $q_w(0, t) = 20$ cm/h: time evolution of the infiltration rate (13a), surface water content and ponded water depth (13b) calculated for the experiments run in the open (solid lines) and bounded (dashed line) columns. t_p is the ponding time.

curve (a)). This may also explain the delay which is observed between the numerical and experimental water content profiles (Figure 9b). This overestimation of h_a can also be seen in Figure 12 for both the flux and the ponding infiltrations. In the latter case, this may explain the poor agreement between the measured and calculated infiltration rates around $t = 0.1$ h (Figure 6b, curve (b)).

This trend can be caused by too small experimental values of the air relative permeability. As a matter of fact, the same numerical simulations were run by using the following linear relation:

$$k_{ra} = \frac{\theta_{ws} - \theta_w}{\theta_{ws} - \theta_{wr}}, \tag{23}$$

which leads to greater values of air conductivity (curve (b) in Figure 4). As an example, the corresponding results are reported in Figures 10b and 11 (curves (b)) for the flux infiltration experiment. As compared to the previous results, a inverse trend is observed: an underestimation of $h_a(t)$ and an overestimation of both t_p (0.18 h) and subsequent cumulative infiltration depths. It appears that the 'experimental truth' is bounded by these two behaviours. No matching relation $k_{ra}(\theta_w)$ has been sought in order to judge the intrinsic predictive capability of the model. The high sensitivity of the results to the air relative permeability values may constitute the strongest limitation for the practical application of the two-phase flow approach, at least based on this concept.

(3) The air pressure profiles (Figure 12) show that the head losses are mainly located inside the wetted region. When air can always escape through the surface (profiles corresponding to $q_w(0, t) = 8.3$ cm/h), the two-phase flow modeling provides an estimate of the viscous resistance of the air flow, which is small in this particular case.

(4) When the air phase is trapped in the medium, its influence on surface parameters is clearly shown in Figure 13: a drastic reduction of t_p of the infiltration rate after ponding (by about 66%) of the steady-state surface water content (by 10%) and an overestimation of the ponding water depth at the surface. Note also that the two-phase flow modeling predicts significant drainage at the surface, allowing the air to escape through it, even though there is ponded water.

6. Discussion and Conclusions

The results presented here have shown the air effects on the water infiltration in a vertical soil column for a broad spectrum of boundary conditions. The main features are as follows:

(i) The differences between the results – both experimental and numerical – corresponding to the experiments run either in the open or in the bounded column, estimate the error committed by predicting water infiltration by the classical unsaturated flow theory, when the soil air flow is impeded.

(ii) When air can freely escape ahead of the wetting front, the viscous resistance of air movement is quite insignificant whatever the surface conditions are, and the one-phase flow approaches seems to be adequate to model the water infiltration (at least for the conditions considered in this study).

(iii) When air can only escape through the surface, the air compression ahead of the wetting front is the major cause of the reduction in the infiltration rates. In this case, the two-phase flow approach should be used to simulate water flows for both ponded and flux conditions applied at the soil surface.

However, although a definite agreement has been observed between the experimental data and numerical results, we are aware that this study poses some key questions.

6.1. HYDRODYNAMIC STABILITY OF WATER MOVEMENT

The analysis of the experimental data has been implicitly based on the assumption that the one-dimensional flow processes were stable in a hydrodynamic sense and that the gradual downward movement of the wetting fronts was not disturbed by the development of a fingering pattern. However, some authors (Hill and Parlange, 1972, White *et al.*, 1976, 1977; Diment, 1982) showed that fingerings can appear during flow in unsaturated porous materials. On the other hand, the stability analysis of two-phase saturated flow in porous media has received considerable attention in petroleum engineering (Saffman and Taylor, 1958; Chuoke *et al.*, 1959; Rachford, 1964; Perkins and Johnston, 1969; Wooding and Morel-Seytoux, 1976; Peters and Flock, 1981). By comparison, the related study of the stability of water flow in unsaturated soils only recently entered soil physics literature. A review indicates that this problem has been analyzed through either the Green and Ampt type-wetting front approach (Raats, 1973; Philip, 1975; Parlange and Hill, 1976) or the linear perturbation technique applied to Equation 16 (Diment, *et al.*, 1982; Diment and Watson 1983) for diffuse wetting fronts.

The main results of these studies are applied here to the experimental data presented above.

For the experiments run in the open column, the analysis of Diment *et al.* (1982) and Diment and Watson (1983) can be used because it has been experimentally shown that the one-phase flow approach is adequate to describe water movements. In this case, the authors clearly show that the infiltration into a homogeneous sand (very similar to the soil used in the present study) leads to stable wetting fronts, at least for initial water contents higher than 0.05 cm^3/cm^3, which is the case in these studies. Note that this trend is consistent with the results given by the analysis of Philip (1975).

For experiments run in the bounded column, frontal instabilities may be theoretically expected (Raats, 1973; Philip, 1975) due to air compression effects ahead of the wetting front. As a matter of fact, by following the analysis proposed by Philip (1975), the water flow is stable if it is assisted by the water pressure gradient behind the wetting front. For a homogeneous soil satisfying the Green and Ampt assumptions, this can be written as

$$h_a(t) - h_{cf} - h_w(0, t) < 0, \tag{24}$$

where $h_a(t)$ is the mean air pressure head ahead of the wetting front $z_f(t)$, h_{cf} is the capillary pressure head at $z_f(t)$, and $h_w(0, t)$ is the water pressure head at the soil surface.

Applying this criterion to the ponded infiltration experiment, with $h_w(0, t) =$ 2.3 cm and h_{cf} given by (Neuman, 1976):

$$h_{cf} = \int_{h_{cn}}^{0} k_{rw}\, \mathrm{d}h_c = 14.5 \text{ cm}$$

of water, leads to $h_a(t) < 16.8$ cm of water. Because this value is not really significantly different from the measured one (see Figure 7), it may be speculated that the water flow was more or less in a neutral stability state throughout the whole experiment. It should be noted that the complete numerical treatment of the simultaneous water and air equations by perturbation techniques for such a case, seems very complicated (Diment and Watson, 1983) even intractable. However, these authors mentioned a simplified modeling of this problem (Equation 16) by the use of an appropriate boundary condition transformation: at the time step of calculation, the surface pressure head is reduced by an amount equal to the calculated air pressure change before the air escape through the surface and by the air entry value h_{ae} after. No instability was predicted for the examples these authors have considered.

On the other hand, wetting-front instabilities may be expected during the early stages of infiltration under flux conditions because $h_w(0, t)$ is significantly less than $h_a(t) - h_{cf}$ and inequality (24) is not satisfied. This makes the experimental results (Figures 8 and 9) questionable for times of less than 0.1 h. Nevertheless, this analysis tends to show that the experimental data used as tests of the numerical modeling are not affected very much by instabilities problems, even for expected unstable flows. This is probably due to a high initial water content ($\theta_{wn}(z) \geqslant 0.08$ cm^3/cm^3) which tends to damp out possible instabilities.

6.2. PERTINENCE OF THE RELATIVE PERMEABILITY CONCEPT

Although no significant deviation from Darcy's law was observed here for both the air and water movements, questions arise nowadays about the validity of this conceptual approach in studying multiphase flows in porous media taken in a more general sense. While both experimental verifications and theoretical justifications of Darcy's law have been extensively reported in the literature for a single fluid, its extension to multiphase flows through the concepts of capillary pressure and relative permeabilities as a function of saturation have raised questions in cases such as dispersed phase flows and instantaneous imbibition (Legait and Jacquin, 1984). Because only empirical verifications are possible at this time, a great effort is needed to provide a theoretical background for the equations describing multiphase flows in porous media. This feeling has been enhanced here by the strong sensitivity of the numerical solutions to the air-related permeability values, mainly close to water saturation.

Should more sophisticated measurement techniques and experimental devices be developed in order to apply the existing conceptual models in a predictive way, or should other theories and models be developed (i.e., Marle, 1984) to interpret the data as they are? Obtaining the answer to this question will probably be of great importance in the near future for those who are interested in problems dealing with transport in porous media.

References

Adrian, D. D. and Franzini, J. B., 1966, Impedance to infiltration by pressure build-up ahead of the wetting front, *J. Geoph. Res.* **71**, 5857–5861.

Bianchi, W. C. and Haskell, E. E., 1966, Air in the vadose zone as it affects water movements beneath a recharge basin, *Water Resour. Res.* **2**, 315–322.

Bond, W. J., 1978, An experimental study of ponded infiltration into simple soil systems, PhD Thesis, University of Sydney, Austrialia.

Boulier, J. F., Touma, J., and Vauclin, M., 1984, Flux-concentration relation-based solution of constant-flux infiltration equation: I – Infiltration into non-uniform initial moisture profiles, *Soil Sci. Soc. Am. J.* **48**, 245–251.

Brustkern, R. L. and Morel-Seytoux, H. J., 1970, Analytical treatment of two-phase flow, *J. Hydraul. Dir. ASCE* **95** (HY12), 2535–2548.

Brutsaert, W., 1970, Immiscible multiphase flow in ground water hydrology: a computer analysis of the well flow problem, PhD Thesis, Colorado State University, Fort Collins.

Chuoke, R. L., Van Meurs, P., and Van der Poel, C., 1959, The instability of slow, immiscible, viscous liquid-liquid displacements in permeable media, *Trans. AIME* **216**, 188–194.

Curtis, A. A. and Watson, K. K., 1980, Numerical analysis of infiltration into a sand profile bounded by a capillary fringe, *Water Resour. Res.* **16**, 365–371.

Cushman, J. H., 1983, Nonstandard finite element analysis of immiscible displacement *Soil Sci.* **135**, 135–142.

Diment, G., 1982, Analysis of wetting front instability in unsaturated porous materials, PhD Thesis, University of New South Wales, Sydney, Australia.

Diment, G. A., Watson, K. K., and Blennerhassett, P. J., 1982, Stability analysis of water movement in unsaturated porous materials. 1 – Theoretical consideration, *Water Resour. Res.* **18**, 1248–1254.

Diment, G. A. and Watson, K. K., 1983, Stability analysis of water movement in unsaturated porous materrials. 2 – Numerical Studies, *Water Resour. Res.* **19**, 1002–1012.

Dixon, R. M. and Linden, D. R., 1972, Soil air pressure and water infiltration under border irrigation, *Soil Sci. Soc. Am. Proc.* **36**, 948–953.

Douglas, J., Peacemen, D. W., and Rachford, H. H., 1959, A method for calculating multi-dimensional immiscible displacement, *Petrol. Trans. AIME* **216**, 297–308.

Free, G. R. and Palmer, V. J., 1940, Inter-relationship of infiltration, air movement and pore size in graded silica sand, *Soil Sci. Soc. Am.* **5**, 390–398.

Green, D. W., Dabiri, H., and Weinaug, C. F., 1970, Numerical modeling of unsaturated groundwater flow and comparison of the model to a field experiment, *Water Resour. Res.* **6**, 862–873.

Haverkamp, R. and Vauclin, M., 1979, A note on estimating finite difference interblock hydraulic conductivity values for transient unsaturated flow problems, *Water Resour. Res.* **15**, 181–187.

Hill, D. E. and Parlange, J. Y., 1972, Wetting front instability in layered soils, *Soil Sci. Soc. Am. Proc.* **36**, 697–702.

Horton, R. E., 1940, An approach toward a physical interpretation of infiltration capacity, *Soil Sci. Soc. Am. Proc.* **5**, 399–417.

Legait, B. and Jacquin, C., 1984, Ecoulements diphasiques en milieu poreux: convergence des phénomènes microscopiques et macroscopiques, *Ann Mines* **5–6**, 57–62.

Linden, D. R., Dixon, R. M., and Guitjens, J. C., 1977, Soil air pressure under successive border irrigations and simulated rain, *Soil Sci.* **124**, 135–139.

MacWhorter, D. B., 1971, Infiltration affected by flow of air, Hydrol. Paper 49, Colorado State University, Fort Collins.

Marle, C. M., 1984, Les écoulements polyphasiques en milieu poreux: de l'échelle des pores à l'échelle macroscopique, *Ann. Mines* **5–6**, 51–56.

Mieri, D., 1981, Two-phase flow simulation of air storage in an aquifer, *Water Resour. Res.* **17**, 1360–1366.

Morel-Seytoux, H. J. and Khanji, J., 1974, Derivation of an equation of infiltration, *Water Resour. Res.* **10**, 795–800.

Morel-Seytoux, H. J., 1982, Analytical results for prediction of variable rainfall infiltration, *J. Hydrol.* **59**, 209–230.

Nakano, Y., 1981, A traveling wave solution to the problem of simultaneous flow of water and air through homogeneous porous media, *Water Resour. Res.* **17**, 57–64.

Neuman, S. P., 1976, Wetting front pressure head in the infiltration model of Green and Ampt, *Water Resour. Res.* **12**, 564–566.

Noblanc, A. and Morel-Seytoux, H. J., 1972, Perturbation analysis of two-phase infiltration, *J. Hydraul. Div. ASCE* **98** (HY9), 1527–1541.

Parlange, J. Y. and Hill, D. E., 1976, Theoretical analysis of wetting front instability in soils, *Soil Sci.* **122**, 236–239.

Parlange, J. Y. and Hill, D. E., 1979, Air and water movement in porous media: compressibility effects, *Soil Sci.* **127**, 257–263.

Parlange, J. Y., Braddock, R. D., and Simpson, R. W., 1982, Optimization principle for air and water movement, *Soil Sci.* **133**, 4–9.

Peck, A. J., 1965a, Moisture profile development and air compression during water uptake by bounded porous bodies. 2 – Horizontal columns, *Soil Sci.* **99**, 327–334.

Peck, A. J., 1965b, Moisture profile development and air compression during water uptake by bounded porous bodies. 3 – Vertical columns, *Soil Sci.* **100**, 44–51.

Perkins, T. K. and Johnston, O. C., 1969, A study of immiscible fingering in linear models, *Soc. Pet. Eng. J.*, 39–45.

Peters, E. J. and Flock, D. L., 1981. The onset of instability during two-phase immiscible displacement in porous media, *Soc. Pet. Eng. J.* 249–258.

Philip, J. R., 1969, Theory of infiltration, *Adv. Hydrosci.* **5**, 216–296.

Philip, J. R., 1973, On solving the unsaturated flow equation. 1 – The flux-concentration relation, *Soil Sci.* **116**, 328–335.

Philip, J. R., 1975, Stability analysis of infiltration. *Soil Sci. Soc. Am. Proc.* **39**, 1042–1049.

Phuc, L. V. and Morel-Seytoux, H. J., 1972, Effect of soil air movement and compressibility on infiltration rates, *Soil Sci. Soc. Am. Proc.* **36**, 237–241.

Powers, W. L., 1934, Soil water movement as affected by confined air, *J. Agric. Res.* **49**, 1125–1133.

Raats, P. A. C., 1973, Unstable wetting fronts in uniform and non-uniform soils, *Soil Sci. Soc. Am. Proc.* **37**, 681–685.

Rachford, H. H. Jr., 1964, Instability in water flooding oil from water-wet porous media containing connate water, *Trans. AIME* **231**, 133–148.

Rubin, J. and Steinhardt, R., 1963, Soil water relations during rain infiltration. I – Theory, *Soil Sci. Soc. Am. Proc.* **27**, 246–251.

Saffman, P. G. and Taylor, G. I., 1958, The penetration of a fluid into a porous medium or Hele–Shaw cell containing a more viscous liquid, *Proc. Roy. Soc.* **A245**, 312–329.

Sonu, J. and Morel-Seytoux, H. J., 1976, Water and air movement in a bounded deep homogeneous soil, *J. Hydrol.* **29**, 23–42.

Starr, J. L., De Roo, H. C., Frink, C. R., and Parlange, J. Y., 1978, Leaching characteristics of a layered field soil, *Soil Sci. Soc. Am. J.* **42**, 386–391.

Touma, J., 1984, Etude critique de la caractérisation hydrodynamique des sols non saturés: Rôle de l'air, influence de l'écoulement multidimensionnel de l'eau, Docteur ès-Sciences Thesis, Université Scientifique et Médicale et Institut National Polytechnique de Grenoble.

Vachaud, G. and Thony, J. L., 1971, Hysteresis during infiltration and redistribution in a soil column at different initial water contents, *Water Resour. Res.* **9**, 111–127.

Vachaud, G., Vauclin, M., Khanji, D., and Wakil, M., 1973, Effects of air pressure on water flow in an unsaturated stratified vertical column of sand, *Water Resour. Res.* **9**, 160–173.

Vachaud, G., Gaudet, J. P., and Kuraz, K., 1974, Air and water flow during ponded infiltration in a bounded column of soil, *J. Hydrol.* **22**, 89–108.

Van Genuchten, M. Th., 1980, A closed-form equation for predicting the hydraulic conductivity of unsaturated soils, *Soil Sci. Soc. Am. J.* **44**, 892–898.

Vauclin, M., 1971, Effects dynamiques sur la relation succion-teneur en eau lors d'écoulements en milieu non saturé, Docteur Ingénieur Thesis, Université Scientifique et Médicale de Grenoble.

Watson, K. K., 1966, An instantaneous profile method for determining hydraulic conductivity of unsaturated porous material, *Water Resour. Res.* **2**, 709–715.

Watson, K. K. and Curtis, A. A., 1975, Numerical analysis of vertical water movement in a bounded profile, *Aus. J. Soil Res.* **13**, 1–11.

White, I., Colombera, P. M., and Philip, J. R., 1976, Experimental study of wetting front instability induced by sudden change of pressure gradient, *Soil Sci. Soc. Am. J.* **40**, 824–829.

White, I., Colombera, P. M., and Philip, J. R., 1977, Experimental studies of wetting front instability induced by gradual change of pressure gradient and by heterogenous porous media, *Soil Sci. Soc. Am. J.* **41**, 483–489.

Wilson, L. G. and Luthin, J. N., 1963, Effect of air flow ahead of the wetting front on infiltration, *Soil Sci.* **96**, 136–143.

Wooding, R. A. and Morel-Seytoux, H. J., 1976, Multiphase fluid flow through porous media, *Ann. Rev. Fluid Mech.* **8**, 233–274.

Youngs, E. G. and Peck, A. J., 1964, Moisture profile development and air compression during water uptake by bounded porous bodies, *Soil Sci.* **98**, 290–294.